DIVERGENCE FREE SYNTHETIC EDDY METHOD FOR EMBEDDED LES INFLOW BOUNDARY CONDITIONS

R. Poletto, A. Revell, T. Craft, N. Jarrin[1]
School of Mechanical Aerospace and Civil Engineering
University of Manchester, Manchester, UK
ruggero.poletto@postgrad.manchester.ac.uk

ABSTRACT

A new inlet treatment for embedded LES is here proposed. The method, based on the SEM proposed by [1], satisfies the divergence free condition of the velocity field, and hence reduces the pressure fluctuations present in the downstream flow close to the inlet with the original SEM. Results compare the new method against the SEM and the VORTEX method, introduced by [2], for a plane channel flow, showing that the proposed scheme produces fairly realistic inlet turbulence, and hence requires a shorter development length compared to the other two schemes.

INTRODUCTION

One of the challenges in performing Large Eddy Simulations (LES) of turbulent flows is the prescription of a suitable velocity field at flow inlets. In most cases these should, ideally, correspond to a suitably realistic unsteady flow field; yet at the same time one also wants them to be reasonably cheap to generate. These requirements hold both for full LES applications, and for RANS/LES hybrid approaches, where 'inlet' conditions for the LES region must be generated from the RANS solution. It is well known that simply imposing random fluctuations on top of a mean velocity field at an inlet will result in a long development length before the flow reaches what might be considered a realistic turbulent state, and so a number of alternative methods have been developed, aimed at providing more realistic representations of inlet turbulence.

Ref [1] developed the Synthetic Eddy Method (SEM) as a quasi-particle based method to generate synthetic turbulence conditions. The method essentially involves the superposition of a (large) number of random eddies, with some control placed on their statistical properties, which are convected through a domain of rectangular cross-section, such as that shown in Fig. 1. The resultant, time-dependent, flow-field from a cross-section of this SEM domain is extracted and imposed as inlet conditions for the LES. Using this approach [1] found that LES of a channel flow at $Re_\tau = 395$ required a distance of around 10–12 channel half-widths to become fully-developed. Some further improvements were achieved by [3], by specifically tuning the shape functions associated with the eddy representations for a channel flow. Although they did report a decrease in the required development length, the form adopted would appear to be rather specific to the application.

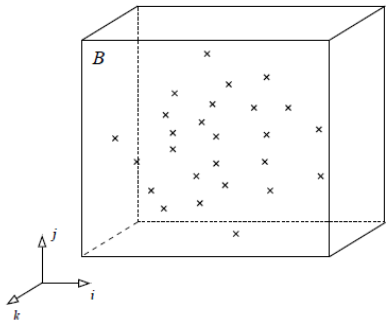

Figure 1. Schematic of the SEM method: the eddies (velocity fluctuations) are generated and convected through an eddy box.

One of the perceived weaknesses of the above SEM methods is that the imposed inlet flow-field does not satisfy the divergence-free condition. As a consequence of this the LES tends to introduce significant pressure fluctuations close to the inlet (in order to adapt the velocity field to something that does satisfy continuity), and this adds to the required development length. In the present work, we therefore explore a method of extending the SEM approach in order to produce a suitable inlet velocity field that does satisfy continuity.

THE DIVERGENCE FREE SEM (DF-SEM)

The DF-SEM is based on the previous version proposed by [1] and [4], with the main difference being the way the velocity fluctuations associated with the eddies are defined. In the SEM these come from the following:

$$\mathbf{u}'(\mathbf{x}) = \frac{1}{\sqrt{N}} \sum_{k=1}^{N} a_{ij} \varepsilon_j^k f_\sigma(\mathbf{x} - \mathbf{x}^\mathbf{k}) \qquad (1)$$

where N is the number of eddies introduced into the SEM domain, $\mathbf{x}^k$ is the location of the centre of the kth eddy, $f_\sigma(\mathbf{x})$ is a

[1]Currently at Areva - France

suitable shape function, ε_j^k are random numbers with zero average and $<\varepsilon_j^k\varepsilon_j^k>=1$ which represent the eddies' intensities and a_{ij} are the Lund coefficients as defined by [5]. Although this formulation does allow the desired Reynolds stress field to be prescribed (via the a_{ij} coefficients), the velocity field will not, in general, also satisfy continuity.

In order to ensure that continuity is satisfied, the DF-SEM applies the SEM approach to the vorticity field and then transforms this back to give a resulting velocity field. Equation (1) is thus applied to the vorticity field, in order to generate fluctuations in it. The curl of the vorticity is then related to the velocity Laplacian by

$$\nabla\times\omega' = \nabla(\nabla\cdot\mathbf{u}') - \nabla^2\mathbf{u}' \tag{2}$$

where, obviously, the first term on the right hand side of equation (2) is neglected because of the divergence free condition. The solution of this Poisson equation, achieved by using the Biot-Savart kernel, finally gives the fluctuating velocity field expressed as follows:

$$\mathbf{u}'(\mathbf{x}) = \sqrt{\frac{1}{N}}\sum_{k=1}^{N}\mathbf{K}_\sigma(\frac{\mathbf{x}-\mathbf{x}^k}{\sigma})\times\alpha^k \tag{3}$$

where α^k are random numbers which represent the eddies' intensities and $\mathbf{K}_\sigma(\mathbf{y})$ is the Biot-Savart kernel, which is defined as $\mathbf{K}_\sigma(\mathbf{y}) = \frac{q_\sigma(|\mathbf{y}|)}{|\mathbf{y}|^3}\mathbf{y}$ with $q_\sigma(|\mathbf{y}|)$ a suitable shape function. It is important to remark here that the above Biot-Savart kernel comes from the solution of equation (2) with the assumption of a constant shape length scale σ and shape function q_σ in the x, y and z directions.

REYNOLDS STRESS TENSOR One of the simplest functions chosen for the shape function q_σ is (for $abs\frac{r^k}{\sigma}<1$)

$$\begin{array}{ll} q_\sigma(\frac{r^k}{\sigma}) = B[sin(\pi\frac{r^k}{\sigma})]^2\frac{r^k}{\sigma} & if \quad |\frac{r^k}{\sigma}|<1 \\ q_\sigma(\frac{r^k}{\sigma}) = 0 & elsewhere \end{array} \tag{4}$$

where $r^k=\sqrt{(x-x^k)^2+(y-y^k)^2+(z-z^k)^2}$, σ is the eddy length scale and B is a scaling coefficient, here taken as $B=\sqrt{\frac{15V_b}{16\pi\sigma^3}}$. V_b is the volume of the box the eddies are convected though. In order to examine what the scheme returns for the Reynolds stresses, equation (3) can be manipulated and averaged, giving[2]

$$\begin{aligned} <u'u'> = &<\alpha_2^2><[q_\sigma(\tfrac{r^k}{\sigma})]^2\tfrac{1}{\sigma^2}\tfrac{(z-z^k)^2}{(\frac{r^k}{\sigma})^6}> \\ &+<\alpha_3^2><[q_\sigma(\tfrac{r^k}{\sigma})]^2\tfrac{1}{\sigma^2}\tfrac{(y-y^k)^2}{(\frac{r^k}{\sigma})^6}> \end{aligned} \tag{5}$$

Because of the symmetry of the eddy contributions in the y and z directions, and the scaling of q_σ noted above, the expression in equation (5) can be simplified to give

$$<u'u'> = \frac{<\alpha_3^2>}{2}+\frac{<\alpha_2^2>}{2} \tag{6}$$

[2]Here only results for $<u'u'>$ are reported, though similar expressions are obtained for $<v'v'>$ and $<w'w'>$.

To see how to scale the random numbers α_j^k to give the desired stress anisotropy, it is convenient to work in the principal axes of the stress tensor, where $<\alpha_1^k>$, $<\alpha_2^k>$ and $<\alpha_3^k>$ can be related to the eigenvalues of the Reynolds stress in the principal axes (λ_1, λ_2 and λ_3) by

$$\begin{array}{l} \lambda_1 = \frac{1}{2}(<\alpha_2^2>+<\alpha_3^2>) \\ \lambda_2 = \frac{1}{2}(<\alpha_3^2>+<\alpha_1^2>) \\ \lambda_3 = \frac{1}{2}(<\alpha_1^2>+<\alpha_2^2>) \end{array} \tag{7}$$

As a result, in order to reproduce the stress anisotropy, α_i^k in equation (3) can be taken as

$$\alpha_i^k = (\sqrt{2(k'-\lambda_i)})\varepsilon_i^k \tag{8}$$

where ε_i^k are random numbers having $<\varepsilon_j^k\varepsilon_j^k>=1$.

In order to obtain the stress field in the original reference frame, the α^k must be transformed back from the principal axes frame to the global frame, using a rotational matrix as below:

$$(\alpha^k)^G = R_L^G(\alpha^k)^L \tag{9}$$

where the superscripts ^{L} and ^{G} refer respectively to the local and the global reference systems.

The final equation for the velocity fluctuations is then:

$$\mathbf{u}' = \sqrt{\frac{1}{N}}\sum_{k=1}^{N}\frac{q_\sigma(\frac{r^k}{\sigma})}{(\frac{r^k}{\sigma})^3}\frac{\mathbf{r}^k}{\sigma}\times[R_L^G(\sqrt{2(k'-\lambda_i)}\varepsilon_i^k)^L] \tag{10}$$

TURBULENCE ANISOTROPY CLIPPING

As result of the square root in equation (8), the present method is not capable of reproducing every state of turbulence, since a very high anisotropy may lead to a negative argument of the square root. The limitation implied by equation (8) is that each normal stress must not be greater than the turbulent kinetic energy. To illustrate the restriction this places on the method, Figure 2 shows the Lumley triangle of possible turbulent stress anisotropy states, with the grey region indicating the states for which equation (8) can be applied. The axes of the picture, ξ and η are defined by: $6\eta^2=b_{ii}^2$; $6\xi^3=b_{ii}^3$, where $b_{ij}=\frac{<u_iu_j>}{<u_ku_k>}-\frac{1}{3}\delta_{ij}$ is the non-isotropic part of the Reynolds stress tensor. The grey area refers to the reproducible area: $\sum_{i=1}^3\lambda_i-2\max\{\lambda_1,\lambda_2,\lambda_3\}\geq 0$. In the same plot are indicated the anisotropy states (circles) of the channel flow DNS at $Re_\tau=395$ by [6]. The limitation might, from this, appear to be rather restrictive; comparing to the DNS data available, the fore-mentioned method could only be applied to represent the stresses correctly for $y^+>300$, although further comments on the severity of this will be made below.

In order to apply the above method, a clipping methodology must be applied to the stress anisotropy, and in the present work this has been implemented by conserving the total turbulent kinetic energy required at the inlet, but redistributing the excess of energy in one direction into the other ones when one stress becomes too large to apply equation (8). In practice, in the present channel flow case this means limiting $<uu>$, and correspondingly increasing $<vv>$ and $<ww>$ near the wall. It should also be noted that since the clipping is applied to the

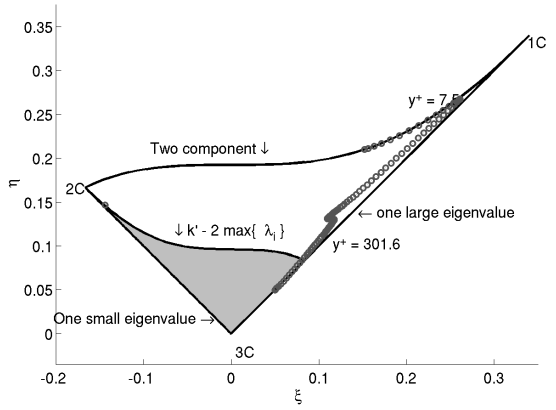

Figure 2. Lumley triangle for the DF-SEM. 1C, one-component; 2C, two-components.

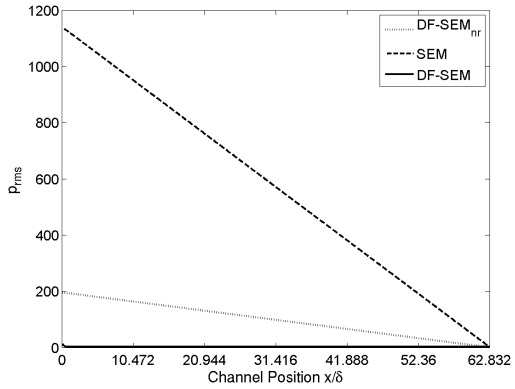

Figure 3. RMS pressure fluctuations with non rescaled SEM and $DF - SEM_{nr}$. DF-SEM refers to an inlet where mass flow rescaling is active.

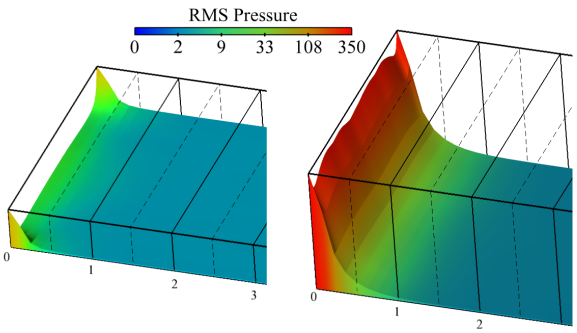

Figure 4. RMS pressure fluctuations close to the inlet with the DF-SEM and the SEM ($y^+ = 395$).

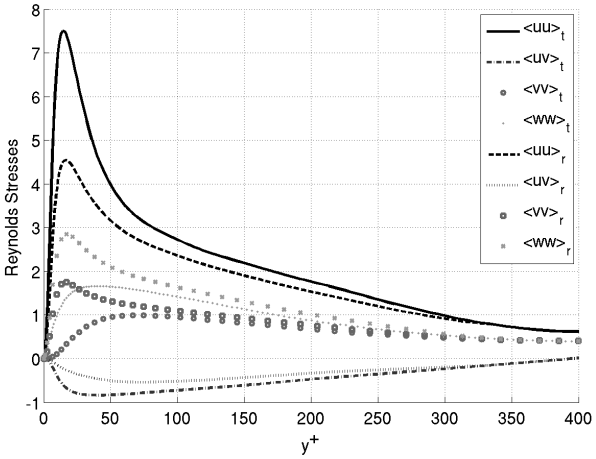

Figure 5. Reynolds stresses clipped by the DF-SEM in a channel flow $Re_\tau = 395$. The superscripts ^{t} and ^{r} refers respectively to the DNS profiles and the clipped ones.

stresses in principal axes, it also affects the shear stress, once the stresses are mapped back to the global reference frame.

Despite the above comments on Figure 2, the results to be presented below will show that although the stress anisotropy clipping is applied over a significant part of the channel inlet, its strongest influence is seen only in the near-wall region with $y^+ < 75$ or so.

MASS FLOW RATE CORRECTION Separate from the above considerations of reproducing the Reynolds stresses, another problem was noted with the SEM and DF-SEM when applied to a wall-bounded internal flow such as the present channel flow. It was noted the stream-wise velocity fluctuations returned by equation (1) or (3) resulted in a non-constant bulk flow rate into the channel (although each eddy has zero mass flow, a numerical sampling of a finite number of them may return a non zero mass flow). This resulted in a time-dependent flow rate along the channel, giving rise to temporal variations in the mean pressure gradient along the channel. As a result, and since the reference pressure is fixed at the channel exit in these simulations, the rms pressure fluctuations show very high levels that decrease linearly with downstream distance (Figure 3), since these fluctuations are dominated by the temporal variation of the mean stream-wise pressure gradient, responding to the time-dependent mass inflow. To avoid the above problem a bulk correction was applied to the inlet velocity profile by simply introducing a rescaling coefficient to ensure the total mass flow rate across the inlet plane remained constant. Numerical simulations showed this rescaling coefficient modified the velocity field by less than 1% in channel flows, and so its effect on the divergence free scheme was deemed negligible. As shown in Figure 3, this correction removed the above problem of a time-dependent mean stream-wise pressure gradient developing. A further benefit of the correction was that it significantly reduced the required computational time for the simulations. The CodeSaturne solver employed here uses the SIMPLER pressure-velocity coupling, and the continually changing bulk pressure gradient along the channel resulted in a large number of iterations being required

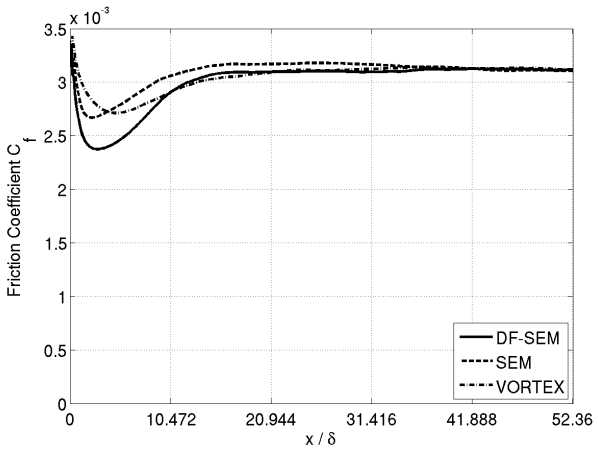

Figure 6. Friction coefficient development along the channel using DNS inlet stresses.

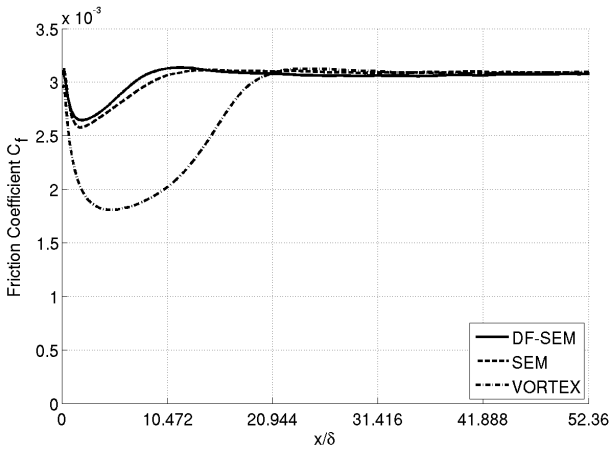

Figure 7. Friction coefficient development along the channel using RANS inlet stresses.

to solve the pressure correction equation. With a constant inlet mass flow many fewer iterations were required to achieve convergence.

Having removed the pressure fluctuations associated with imposing a time-dependent mass inflow, a beneficial feature of the DF-SEM in the near inlet region can clearly be identified. Figure 4 shows rms pressure fluctuation levels along the channel, close to the inlet, at around $y^+ = 395$ using the SEM and DF-SEM (both now employing the above inlet mass flow correction). The SEM shows high levels of fluctuations locally around the inlet. These arise since the imposed inlet velocity fluctuations do not satisfy continuity, and significant pressure fluctuations therefore develop at the inlet as the LES must produce a divergence-free velocity field in the first cell of the domain. The DF-SEM, which produces a divergence-free inlet velocity field, results in much smaller inlet pressure fluctuations, with relatively high values only very close to the periodic boundaries of the domain (it is believed these may be due to some detail of the periodic boundary condition implementation).

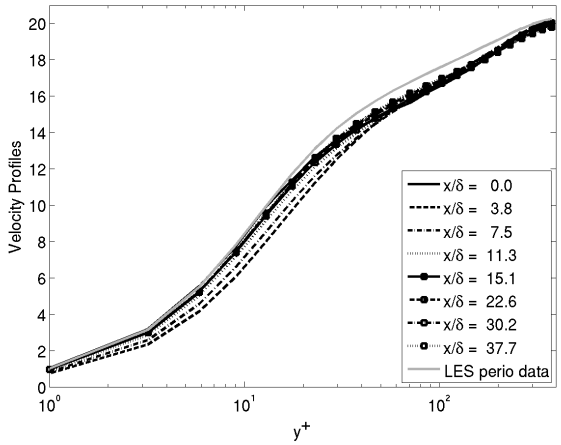

Figure 8. Velocity profiles using the DF-SEM.

CHANNEL FLOW RESULTS

Channel flow simulations have been carried out to test the new method against some other commonly used ones. In the results presented below, DF-SEM refers to the divergence-free SEM method outlined above, whilst SEM refers to the original scheme of [4]. In both cases the bulk mass flow correction described above has been applied to the scheme. The third set of results correspond to simulations employing the VORTEX method of [2]. The simulations have been carried out for a channel flow with $Re_\tau = 395$. The size of the domain was $20\pi \times 2 \times \pi$, which was covered by a mesh of $500 \times 46 \times 82$ cells, with $y^+ \approx 1$ at the walls. The inlet conditions were generated by the three methods noted above, using DNS data for the turbulent stress levels. Figure 5 shows the Reynolds stress profiles from DNS and those employed in the DF-SEM approach, clearly indicating the effect the above clipping algorithm has on the inlet profiles from the DF-SEM. Exact stresses are reproduced only for $y^+ > 300$, although the clipping is relatively modest until $y^+ > 75$, where the DNS begins to show highly anisotropic turbulence.

FRICTION COEFFICIENT The development of the friction coefficient along the channel is a convenient parameter to compare the performance of the three methods tested. The general behavior, shared among all the simulations, and shown in Figure 6, is a sudden drop of C_f, followed by a recovery to the fully-developed value give by the LES scheme. Both the initial drop and the recovery rate are highly influenced by the synthetic turbulence used to define the inlet. The DF-SEM results in the largest initial drop among the tested methods but, on the other hand, has the shortest recovery length, whereas the SEM exhibits an overshoot of C_f before gradually returning to the final level. The VORTEX methodology also shows a rather slow recovery, even though its initial drop is the smallest among the methods tested.

In order to show more clearly the positive influence of the DF-SEM, a second set of channel flow simulations has been performed, this time with the inlet stresses taken from a RANS simulation (using the k-ω SST Eddy Viscosity Model).

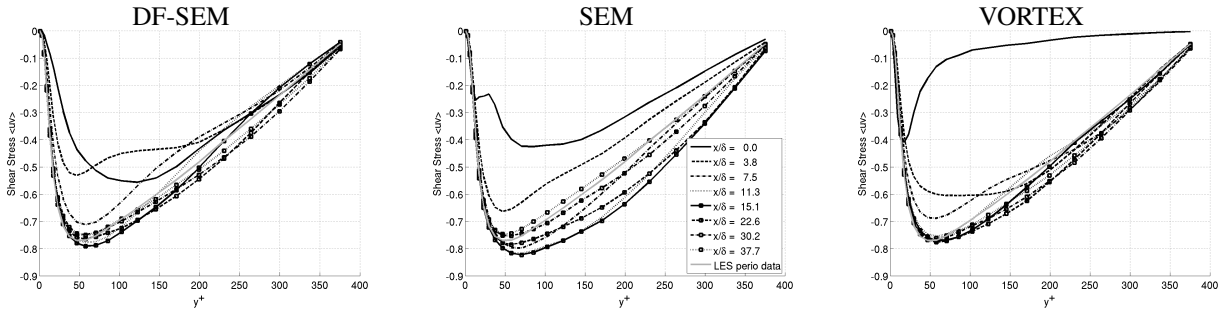

Figure 9. $< uv >$ profiles at selected streamwise locations using the DF-SEM, SEM and VORTEX inlet conditions.

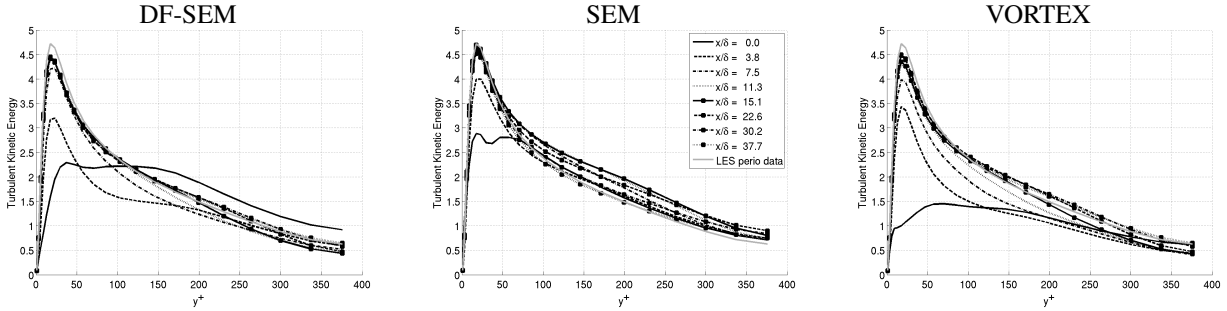

Figure 10. k profiles at selected streamwise locations using the DF-SEM, SEM and VORTEX inlet conditions.

While the VORTEX method performance in this case appears to be significantly worsened, the DF-SEM substantially maintains the same development length, as does the SEM. Although the similarity in the DF-SEM behaviour in the two cases is encouraging, it may be partly due to the limitation in turbulence anisotropy reproduction mentioned earlier. The clipping of the DNS levels may result in the stresses actually imposed in the first case not being all that different from those used in the second.

VELOCITY PROFILES Figure 8 shows mean velocity profiles at a selection of stream-wise locations from the simulation using the DF-SEM inlet conditions. There is a small underestimation of the velocity for $y^+ < 40$ and $x/\delta < 11$, corresponding to the zone where the friction coefficient shows a dip towards the start of the channel. It should also be noted that it is in this near wall region where the clipping of the stress anisotropy has a significant effect on the Reynolds stresses employed in the DF-SEM. However, overall the profiles show little variation along the channel length.

TURBULENT SHEAR STRESS Profiles of the turbulent shear stress, shown in Figures 9, are particularly interesting. Bearing in mind that the DF-SEM does not reproduce the precise state of turbulence for $y^+ < 300$, the inlet shear stress magnitude is always under estimated, as shown in Figure 9. However, for $y^+ > 250$, $< uv >$ recovers almost instantaneously with the DF-SEM, and even over the rest of the channel the profiles beyond $x/\delta \approx 10$ are very close to the fully developed LES data.

The SEM, on the other hand, exhibits a rather long recovery, and the overshoot noticed in the friction coefficient can also clearly be seen in the $< uv >$ profiles. The VORTEX method has a very peculiar behavior: a very low inlet shear stress is provided by the method itself, consistent with the fact that the method applies the fluctuations in the x direction using a separate equation (so u and v are not correlated). At the first downstream cell ($x/\delta = 0$) only for $y^+ < 20$ is there any agreement with the fully developed values. Nevertheless, the method is able to recover rapidly from this initial underestimation and at $x/\delta = 3.8$ the prediction of the shear stress is consisted with the periodic solution for $y^+ > 200$ as well. The remaining region, $20 < y^+ < 200$ develops over a longer distance, leading to the lengthy recovery of C_f noted earlier.

TURBULENT KINETIC ENERGY Figure 10 shows profiles of the turbulent kinetic energy along the channel using the three different inlet treatments. The VORTEX methodology introduces low inlet turbulence levels, consistent with the shear stress seen in Figure 9. For both the DF-SEM and the SEM it seems that part of the energy is dissipated at the beginning of the channel (since the profile at the inlet would give a peak corresponding roughly to the LES peak), and then is recovered as the flow develops along the channel. In all three cases the energy profiles reach their fully-developed values at approximately $\frac{x}{\delta} = 10$ and again, as already noticed, the SEM exhibits a kind of overshoot which affects its performance.

FOURIER ANALYSIS To shed further light on the comparison between the different inlet generation methods, a Fourier analysis of the inlet velocity signal has been performed. The selected locations where the spectral analysis

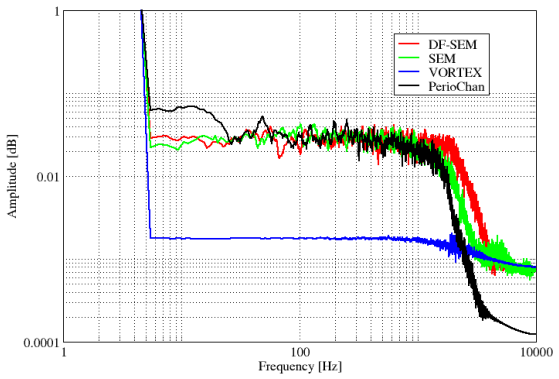

Figure 11. Fourier analysis of U at $y^+ = 390$.

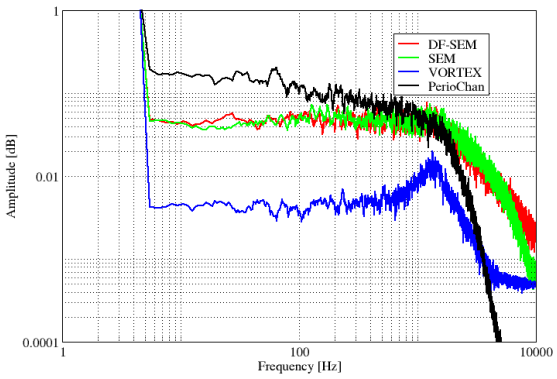

Figure 12. Fourier analysis of U at $y^+ = 39.5$.

has been performed are near the centreline, at $y^+ = 390$, and closer to the wall at $y^+ = 39.5$, shown in Figures 11 and 12.

Each case is compared to the spectra obtained from a fully-developed LES channel flow calculation. The figures show a significant under predictions of the fluctuations in the VORTEX method at $y^+ = 390$. The SEM shows a strange behavior at high frequency, where a double peak is present. The DF-SEM produces fluctuations with higher frequency than the SEM, mainly because, even though the same eddy length scale is applied to both methods, the precise scales of the fluctuations imposed by the two types of eddies are different (as a result of the different shape functions employed in the two methods).

CONCLUSIONS

The new method described here, based on the existing SEM suggested by [4], allows a synthetic turbulence field to be generated that does satisfy the divergence free condition. This feature, not present in other synthetic turbulence algorithms, helps reduce the length of the required development region at the domain inlet.

Channel flow results demonstrated that, using this method, the friction coefficient recovers to its fully-developed value over a shorter distance than that required using other inlet conditions tested. The shear stress and turbulent kinetic energy profiles also showed the new method performing very well for $y^+ > 250$, although recovering slightly more slowly at smaller y^+ values. This latter feature is believed to be due to the clipping currently employed on the prescribed inlet stress anisotropy levels, and further work is being performed in an attempt to broaden the range of inlet stress levels which the method can reproduce.

REFERENCES

[1] N. Jarrin, R. Prosser, J. Uribe, S. Benhamadouche, and D. Laurence, "Reconstruction of turbulent fluctuations for hybrid RANS/LES simulations using a Synthetic-Eddy method," *International Journal of Heat and Fluid Flow*, vol. 30, pp. 435–442, June 2009.

[2] M. E. Sergent, *Vers une Methodologie de Couplage Entre la Simulation des Grande Echelles et les Modeles Statistiques*. PhD thesis, Ecole Central de Lyon, 2002.

[3] M. Pamiès, P.-É. Weiss, E. Garnier, S. Deck, and P. Sagaut, "Generation of synthetic turbulent inflow data for large eddy simulation of spatially evolving wall-bounded flows," *Physics of Fluids*, vol. 21, no. 4, p. 045103, 2009.

[4] N. Jarrin, S. Benhamadouche, D. Laurence, and R. Prosser, "A synthetic-eddy-method for generating inflow conditions for large-eddy simulations," *International Journal of Heat and Fluid Flow*, vol. 27, pp. 585–593, Aug. 2006.

[5] T. S. Lund, X. Wu, and K. D. Squires, "Generation of turbulent inflow data for Spatially-Developing boundary layer simulations," *Journal of Computational Physics*, vol. 140, pp. 233–258, Mar. 1998.

[6] R. D. Moser, J. Kim, and N. N. Mansour, "Direct numerical simulation of turbulent channel flow up to $\mathrm{Re}_\tau = 590$," *Physics of Fluids*, vol. 11, no. 4, pp. 943–945, 1999.